A Novel Gold-Coated Multimode Fiber Sensor

Eduardo Fontana

***Abstract*—A novel optical-fiber sensor is proposed for use in chemical analysis. The sensor probe is made of a gold-coated multimode optical fiber, configured to exhibit surface plasmon resonance (SPR) when immersed in a wet environment. The proposed detection strategy comprises measurement of the image pattern irradiated by the fiber under monochromatic illumination. A theoretical model is proposed to determine device performance. From computer simulations, it is shown that the proposed configuration and detection strategy allows reaching a 30-fold enhancement in sensitivity relative to that obtained in previous SPR-based versions of the device.**

***Index Terms*—Chemical sensor, fiber sensor, gold, SPR, surface plasmon.**

I. Introduction

OPTICAL sensing of chemical reactions occurring nearby a surface is a valuable tool for determination of the concentration of chemical species within an aqueous medium, as well as for kinetic studies related to the reaction of immobilized molecules and their binding partners in solution, as in optical immunoassays [1]. Amongst several approaches, surface plasmon resonance (SPR) in the Kretschmann prism coupling configuration [2] is perhaps the first optical technique to find a feasible commercial application in the field of *in situ* chemical analysis, without the use of radioactive or fluorescent labeling as in conventional methods [3], [4]. More recently, optical-fiber versions of the technique have been investigated [5]. The proposed design for chemical sensing in a wet environment comprises a multimode fiber of large numerical aperture [5], with a small length of the cladding replaced by a thin film of gold, covered with a chemically sensitive organic layer. Due to the resonance effect, the optical power transmitted through the fiber is partially absorbed, the degree of which is wavelength dependent. Specific reactions on the chemically sensitive layer are translated as changes in the absorption spectrum of the light transmitted through the fiber.

One drawback of the wavelength scan detection scheme proposed [5] is that the resonant absorption is totally integrated upon detection, in turn reducing the potential sensitivity of the device.

In this paper, a theoretical model is developed to determine the intensity distribution of light irradiated by a multimode fiber, designed to exhibit SPR when immersed in a wet environment. From this theoretical model, the potential sensitivity of the wavelength scan detection scheme is estimated. It is shown that using a monochromatic light source and a suitable modification of the probe configuration and accompanying detection strategy it is possible to obtain a 30-fold enhancement in the device sensitivity.

Manuscript received May 21, 2000; revised November 22, 2000. This work was supported under the Conselho Nacional de Desenvolvimento Científico e Tecnológico and under the Financiadora de Estudos e Projetos.

The author is with the Departamento de Eletrônica e Sistemas, CTG/UFPE, Recife PE, Pernambuco 50.740-530 Brazil (e-mail: fontana@npd.ufpe.br).

Publisher Item Identifier S 0018-9480(02)00756-1.

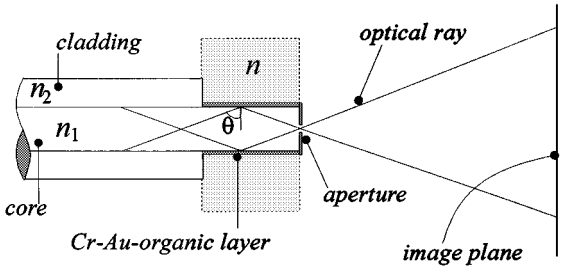

Fig. 1. Proposed design for a fiber chemical sensor employing SPR as the transducing mechanism.

II. SPR on a Multimode Optical Fiber

Fig. 1 illustrates the basic approach proposed in this paper to observe SPR from the light irradiated by a multimode fiber. The core and cladding composing the optical fiber are assumed to have refractive indexes n_1 and n_2, respectively, and the medium surrounding the metal film, usually an aqueous solution, has a refractive index n. At the fiber output end, a portion of the cladding is removed and replaced by a layered structure comprising a Cr adhesion layer approximately 3-nm thick, an Au film 50-nm thick, and a chemically sensitive organic layer [3], [4]. An optical ray propagating down the fiber is assumed to form an angle θ relative to the normal direction to the fiber cylindrical surface. The configuration proposed in this paper uses as detection strategy the measurement of light distribution on the image plane as a route to retrieving information on optical changes occurring on the exposed metal surface, such as those produced by surface chemical reactions. The fiber sensor configuration differs from that studied previously [5] by the addition of a small aperture around the center of the fiber output surface. The aperture can be readily fabricated by vacuum deposition techniques and serves the purpose of blocking skew rays, as well as those meridional rays not crossing the fiber axis at the output surface. The angular range that illuminates the metal surface and effectively makes it through the aperture depends on the core radius and length of metal film, as will be discussed later.

A zeroth-order approximation for the resonance angle θ_{SP} of a surface plasmon (SP) oscillation excited on the exposed portion of the metal surface is given by [2]

$$\theta_{\mathrm{SP}} = \sin^{-1}\left[\frac{1}{n_1}\left(\frac{\varepsilon' n^2}{\varepsilon' + n^2}\right)^{1/2}\right]. \tag{1}$$

TABLE I
SPR PARAMETERS FOR A (SILICA–Cr–Au–AQUEOUS SOLUTION) MULTILAYER STRUCTURE

λ(nm)	n_1 / n_2	$-\varepsilon'_{Cr}$ / $-\varepsilon''_{Cr}$	$-\varepsilon'_{Au}$ / $-\varepsilon''_{Au}$	θ_{SP} [a] (deg)	θ_{SP} [b] (deg)
632.8	1.457	6.46	10.826	—	83.52
	1.391	30.848	0.764		
670	1.456	5.28	13.308	76.75	78.84
	1.390	32.368	0.693		
760	1.454	2.51	19.671	73.97	73.92
	1.388	35.426	0.718		

[a] Calculated using the zero order approximation given by (1).
[b] Calculated from [3] for a (3 nm Cr/50nm Au) bilayer.

In (1) , ϵ' represents the real part of the metal complex permittivity. This parameter is negative when the driving frequency is smaller than the plasma frequency [2]. For a given optical fiber, SPR can be observed if the condition

$$\theta_c < \theta_{\rm SP} < \frac{\pi}{2} \tag{2}$$

is satisfied, where

$$\theta_c = \sin^{-1}\left(\frac{n_2}{n_1}\right) \tag{3}$$

is the critical angle for total internal reflection at the core-cladding interface. Observation of the oscillation also requires the driving electromagnetic field to display an E-field component perpendicular to the glass/metal interface.

The SP resonance angle, calculated within the zeroth-order approximation, for the case of a gold film covering a silica glass substrate is shown in Table I for three distinct wavelengths. Silica and metal optical constants were obtained from [6] and [7], respectively. The external medium is assumed to have a refractive index $n = 1.333$, a value that matches that of pure water [3], thus simulating the fiber operating conditions as a chemical sensor device. Notice that, in the zeroth-order approximation, for the HeNe wavelength of 632.8 nm, (1) does not predict the existence of an SP resonance. Also listed in Table I are the core and cladding refractive indexes of the multimode fiber selected for the design of the sensor device. This fiber, fabricated by 3M Specialty Optics, West Haven, CT, has a silica core having 1-mm diameter and a plastic cladding 40-μm thick, with a numerical aperture of 0.48; the latter translating to a minimum ray propagation angle $\theta_c \approx 72.7^\circ$, thus lower than the resonance angles predicted by the zeroth-order approximation.

Exact values for the resonance angle of the metal-film reflectance function are shown in the rightmost column of Table I. These numbers are calculated using the Fresnel reflection formulation for a Kretschmann prism geometry [3] consisting of a silica–chromium–gold–water multilayer structure for a Cr film 3-nm thick and a gold film 50-nm thick. The chromium underlayer is employed to improve adhesion of gold to glass as described in the literature [3]. It is important to notice that the exact calculation shows that the SP resonance can be observed at the HeNe wavelength of 632.8 nm, and the resonance position should occur around 83.5°, a result not predicted within the zeroth-order approximation.

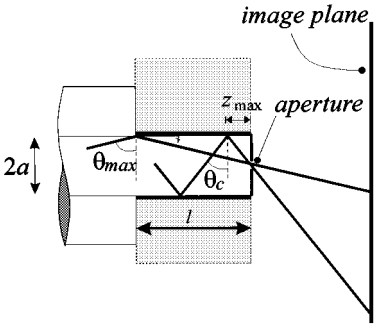

Fig. 2. Geometry of the metallized portion of the fiber sensor.

III. LIGHT IRRADIATED FROM AN OPTICAL FIBER UNDER SPR

A theoretical model was developed and computer simulations were conducted in order to obtain the image pattern that would be expected after a guided light beam emerged from the multimode fiber output end illustrated in Fig. 1. The expected experimental configuration for confirming the simulated results should entail a detection strategy to record the image transmitted through the fiber. This could be done, e.g., by use of a photodiode array placed on the image plane.

A. Design Considerations

In the theoretical model, it is assumed that the Cr–Au bilayer is uniformly coated on a length l over the exposed fiber core of radius a, located near the output end, as illustrated in Fig. 2, and that the fiber is long enough so that points located on distinct axial positions are equivalent and, therefore, subject to illumination by the same angular range guided by the fiber. The output aperture, however, imposes a limitation on the meridional rays that are effectively transmitted to the image plane shown in Fig. 1. The angular range that effectively shines the metal surface can be determined with the help of Fig. 2. Light reflected from the metallized portion located a distance smaller than

$$z_{\max} = a \tan\theta_c \tag{4}$$

cannot be transmitted through the aperture. On the other hand, as shown in Fig. 2, the largest value of the incidence angle θ that reflects on the metal surface and is transmitted to the image plane is given by

$$\theta_{\max} = \tan^{-1}\left(\frac{l}{a}\right). \tag{5}$$

Another design parameter of importance is the number of reflections N_1 undergone by a guided ray propagating with incidence angle θ on the metallized section. This parameter is given by

$$N_1 = \frac{l}{2a\tan\theta}. \tag{6}$$

To avoid broadening the resonance effect and, thus, degrading sensitivity, it is important to restrict this number to a maximum value of one for the ray propagating close to the total internal reflection condition. This imposes an upper limit on the length l of the metal film covering the fiber core. This upper limit can

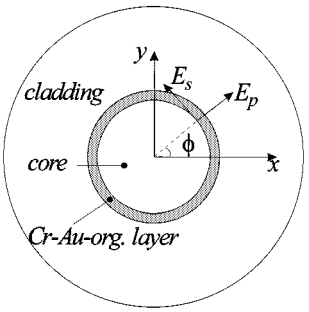

Fig. 3. Fiber cross section and corresponding reference system.

be determined from (6) by imposing the condition $N_1 < 2$ at $\theta = \theta_c$, yielding $l < l_{\max}$ with

$$l_{\max} = 4a \tan \theta_c. \tag{7}$$

From (5), one can conclude that, in order to obtain the maximum angular range reflected from the metal surface and transmitted to the image plane, one has to chose the largest possible length l satisfying (7). Once this requirement has been met, the range of incidence angles can be determined from (5) and (7) yielding

$$\theta_c < \theta < \tan^{-1}(4 \tan \theta_c). \tag{8}$$

For the multimode fiber considered in this paper, $a = 0.5$ mm and $\theta_c = 72.7°$. From (4), one obtains $z_{\max} = 1.6$ mm. From (7), one can choose a maximum length $l_{\max} = 6.42$ mm, thus restricting the angular range reflected from the metal surface and passing through the aperture to $72.7° < \theta < 85.54°$. As can be observed from Table I, this angular range would still enable observing a significant portion of the resonance effect at the HeNe wavelength of 632.8 nm.

B. Intensity Distribution

In the theoretical model developed in this Appendix, a ray propagating at an angle θ relative to the line perpendicular to the cylindrical surface is decomposed into independent polarization components, one with the electric field parallel to the cylindrical surface (referred to as the s-wave component) and the other with the electric field perpendicular to that surface (referred to as the p-wave component), as shown in Fig. 3. As mentioned earlier, SP oscillations can only be excited by the p component of the E-field and, thus, a number of possible image patterns can be generated depending on the input and output polarization conditions imposed on the light beam.

It is assumed that the input beam is focused to the center point of the fiber input flat surface, with an angular range defined by the fiber numerical aperture. Thus, the input beam intensity distribution can be described by a normalized Gaussian profile, as predicted within the paraxial approximation [8], of the form

$$I_0(\theta) = \exp\left[-2\left(\frac{\tan\theta_c}{\tan\theta}\right)^2\right]. \tag{9}$$

As shown in the Appendix, the intensity distribution of the light irradiated from the fiber output can be described in terms of the functions $F_{uu}(\theta)$, $F_{up}(\theta, \phi)$, and $F_{pp}(\theta, \phi)$, given by (A8), (A11), and (A10), respectively. The subscripts refer to the input and output polarization states of the beam. Thus, uu refers to an unpolarized beam launched at the input and directly observed on the image plane. The subscript up refers to an unpolarized input beam, with the output beam passing through an x-analyzer placed between the image plane and the fiber output end. The subscript pp refers to the pattern generated by an x-polarized beam after passage through an x-analyzer.

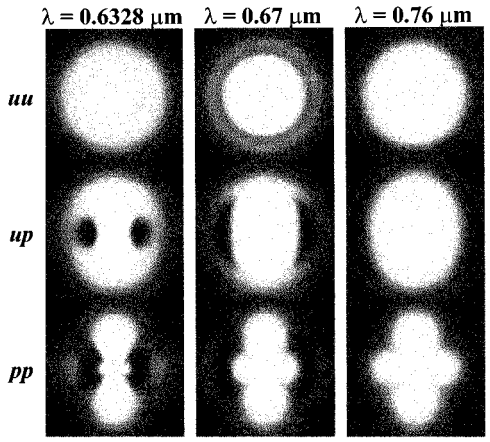

Fig. 4. Intensity patterns of the light irradiated by a fiber sensor under SPR.

Fig. 4 shows the calculated intensity distributions irradiated by the fiber as observed on the image plane at three distinct wavelengths for a metal coated fiber having $l = l_{\max}$ and $a = 0.5$ mm and for the Cr and Au parameters listed in Table I.

As can be noticed from Fig. 4, the uu polarization state produces an image pattern exhibiting a dark ring indicative of the SPR effect. One can notice that the ring radius increases with the wavelength, thus indicating a decrease in the resonance angle $\theta_{\rm SP}$, as expected from Table I. Notice that due to the existence of p- and s-polarization states in the output beam, a weak contrast occurs.

The resonance effect can be enhanced by placing an analyzer along any direction in the image plane. This is shown in the second row of images, labeled up in Fig. 4. The SP resonance is clearly observed with the highest contrast occurring along the $\phi = 0$ azimuth angle, the latter defining the analyzer axis. The effect can be further enhanced in the x-direction for an x-polarized input beam, as shown for the row labeled pp in Fig. 4. However, for a long fiber section prior to the sensitive region, bending would probably brake this condition and the pp pattern would more likely resemble the up pattern shown in Fig. 4.

IV. Sensitivity Considerations

The detection scheme proposed in the literature[5] employs a broad-band light source that is focused down to the fiber sensor input, with the analysis of either the transmitted or reflected optical power wavelength spectrum being used to sense optical changes in the aqueous environment nearby the chemically sensitive surface. In order to compare the potential sensitivities of this scheme with that proposed in this paper, the spectral dependence of the total optical power transmitted through the optical fiber has been calculated for the uu state. A Mathcad computer code was developed to carry out all calculations. The built-in

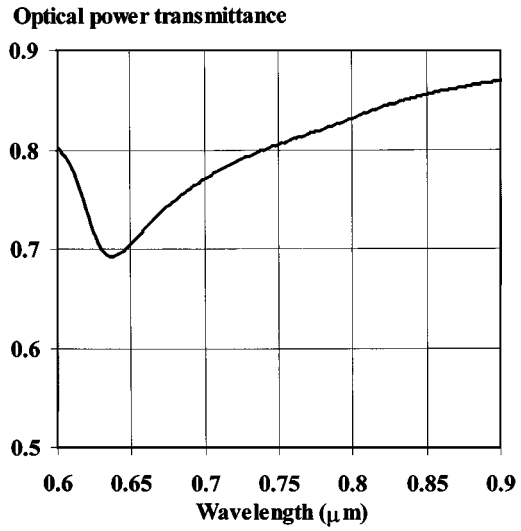

Fig. 5. Wavelength spectrum of the optical power transmittance, as calculated from (9).

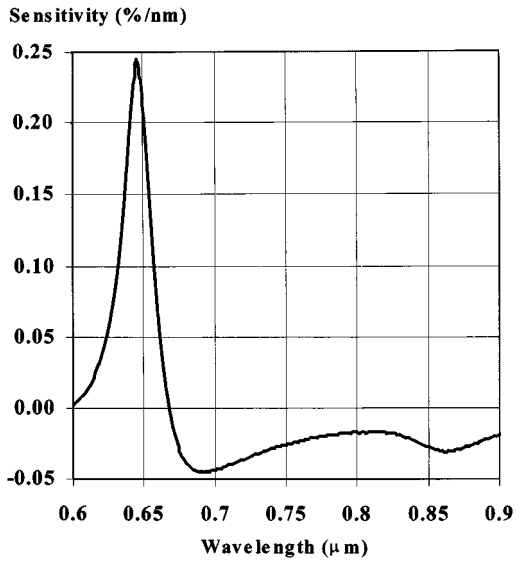

Fig. 6. Wavelength spectrum of the sensitivity of the transmitted optical power to changes in thickness of the organic layer.

cubic spline fitting procedure, available in the Mathcad application, was used to generate continuous functions for the optical constants of Au and Cr, tabulated in the literature [7]. The total optical power transmitted through the aperture can thus be calculated from the expression

$$T(\lambda) = \frac{\int_{\theta_c}^{\pi/2} F_{uu}(\theta) \cos\theta d\theta}{\int_{\theta_c}^{\pi/2} I_0(\theta) \cos\theta d\theta} \tag{10}$$

where I_0 and F_{uu} are given in (9) and (A8), respectively.

In order to calculate the function F_{uu} used in (10), the Fresnel reflection formulation was used to derive the p- and s- wave reflectivities for a silica/chromium/gold/organic layer/water multilayer geometry [3]. The organic layer, assumed to have a refractive index of 1.5, was set to have an initial thickness of 10 nm. A value of 1.333 was adopted for the refractive index of the external aqueous medium and thickness values of the Cr and Au metal films were those listed under Table I. The organic layer parameters were chosen so as to represent the figures typically found in most immunosensor applications[1], [3]–[5]. The metal film length was assumed to satisfy (7) so that F_{uu} was calculated by setting $N_1 = 1$ in (A8).

Fig. 5 shows the wavelength spectrum of the optical power transmitted through the optical fiber. Maximum resonance absorption occurs in a wavelength range near 0.64 μm. In Fig. 6, the sensitivity of this detection approach is plotted from the calculated change in transmitted signal for a 1-nm change in the organic layer thickness. As can be noticed from that plot, the wavelength scan detection scheme produces a curve that is sharply peaked near 0.64 μm with a maximum relative change of approximately 0.25% per nanometer added to the organic layer.

The measurement approach proposed in this paper to maximize device sensitivity can be outlined with the help of Figs. 2 and 3. Assuming a monochromatic unpolarized beam launched at the fiber input, and considering the coordinate system defined in Fig. 3, the detection system would comprise an x-analyzer placed after the fiber output surface and a linear photodiode array placed on the image plane illustrated in Fig. 2. The photodiode array axis should be aligned parallel to the analyzer axis and located on the plane $y = 0$ so as to record the intensity distribution along that plane. This arrangement would have the benefit of preserving the spatial nature of the SPR effect as a route to developing a highly sensitive chemical sensor.

To determine the improvement that can be achieved by use of this detection strategy, a Mathcad computer simulation was conducted to determine the changes produced on the intensity pattern caused by a small increment in thickness of the organic layer covering the metal surface. Assuming that the fiber sensor is designed with a length of metal film satisfying (7), the spatial distribution of light intensity on the plane $y = 0$ can be obtained from (A11) for $N_1 = 1$ and setting $\phi = 0$ (or π), i.e.,

$$F_{up}(\theta, \phi = 0) = |r_p(\theta)|^2 E_0^2 \tag{11}$$

where E_0 and r_p are the field amplitude at the fiber input and the p-wave reflectivity of the multilayer structure, respectively, as described in the Appendix. By use of (11), a numerical procedure was executed to calculate the spectral dependence of the angle $\theta_{\max}$ where maximum intensity variation would occur for a given increment in the organic layer thickness. This angle corresponds approximately to the point of maximum slope of the p-wave reflectance function on the right-hand side (RHS) of (11), with the exact value being dependent on the input distribution of the E-field. As in the calculations that led to the results shown in Fig. 6, the organic layer thickness increment was set at 1 nm, with the corresponding maximum intensity change being calculated for each wavelength.

The plot shown in Fig. 7 exhibits the spectral dependence of the sensitivities calculated from (11) for the cases $E_0^2 = 1$ and $E_0^2 = l_0(\theta)$, corresponding to a uniform and Gaussian distribution of incidence angles launched through the fiber, respectively. As shown in that plot, use of the Gaussian distribution results in a slight decrease in sensitivity, relative to that calculated for a uniform input distribution. Notwithstanding, a direct

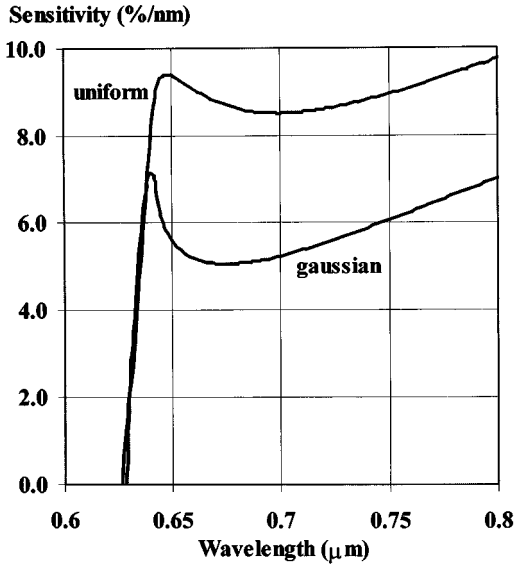

Fig. 7. Wavelength spectra of the fiber device sensitivity as determined from the light distribution on the image plane.

comparison of the curve shown in Fig. 6 with that obtained for a Gaussian distribution in Fig. 7 shows that the detection approach proposed in this paper is up to 30 times more sensitive than the conventional wavelength scan detection scheme. One second important feature that can be observed from the plot shown in Fig. 7 is that the device could be made to operate at a given preset wavelength within a broad spectral range, a feature that cannot be adopted in the conventional detection approach. For instance, considering a Gaussian input distribution, the minimum sensitivity observed in Fig. 7 is about 5%/nm at 0.67 μm, which is still about 20 times larger than the maximum value that can be detected from changes in the total transmitted optical power.

V. Conclusions

In this paper, a theoretical model has been developed to determine the intensity distribution of light irradiated by a multimode fiber, designed to exhibit SPR when immersed in a wet environment. From this model, an improved fiber sensor configuration has been proposed with a novel detection strategy for recording the spatial resonance arising within the light irradiated from the fiber device. It has been shown that these modifications can enhance device sensitivity up to 30 times relative to that currently attainable with the wavelength scan detection scheme. Further work on this field will comprise construction of the fiber sensor here proposed, as well as experimental characterization of device performance.

Appendix

To determine the output intensity of the light transmitted through the fiber, the polarization state for the input field is assumed of the form

$$\tilde{E}_{xy} = \begin{pmatrix} E_x \\ E_y \end{pmatrix}.$$

In the rotated reference system shown in Fig. 3, the E-field can be obtained by use of the matrix transformation

$$\tilde{E}_{ps} = \tilde{R}(\phi)\,\tilde{E}_{xy} \tag{A1}$$

where

$$\tilde{R}(\phi) = \begin{pmatrix} \cos\phi & \sin\phi \\ -\sin\phi & \cos\phi \end{pmatrix}.$$

On the nonmetallized portion of the fiber, the guided field undergoes total internal reflection. Under this condition, the p and s reflection coefficients both have a unit amplitude. Thus, the relationship between reflected and incident fields at the nth reflection can be expressed in matrix form as

$$\tilde{E}_{ps}^{\langle n\rangle} = \tilde{W}_0 \tilde{E}_{ps}^{\langle n-1\rangle} \tag{A2}$$

where the elements of the column vector in the left-hand side (LHS) of (A2) are the E-field components in the ps reference system after the nth reflection and

$$\tilde{W}_0 = \begin{pmatrix} e^{j\gamma_p} & 0 \\ 0 & e^{j\gamma_s} \end{pmatrix} \tag{A3}$$

with γ_p and γ_s representing the phase shifts introduced on the p- and s-field components, respectively, after reflection. On the metallized portion of the fiber, the p- and s-field components undergo reflections. A transformation relation similar to (A2) holds for the reflected and incident fields on the metallized region, and can be defined by the matrix

$$\tilde{W}_1 = \begin{pmatrix} |r_p|\, e^{j\delta_p} & 0 \\ 0 & |r_s|\, e^{j\delta_s} \end{pmatrix} \tag{A4}$$

where r_p, δ_p, r_s, and δ_s are the amplitudes and phases associated with the p- and s- field components, respectively.

Assuming that each ray undergoes N_0 and N_1 reflections on the nonmetallized and metallized portions of the fiber, respectively, the output field in the ps reference system can be written as

$$\tilde{E}_{ps}^{\langle N_0+N_1\rangle} = \tilde{W}\tilde{E}_{ps}^{\langle 0\rangle}$$

with

$$\tilde{W} = e^{j\Delta_p} \begin{pmatrix} |r_p|^{N_1} & 0 \\ 0 & |r_s|^{N_1} e^{j\Delta} \end{pmatrix} \tag{A5}$$

where

$$\begin{aligned} \Delta &= \Delta_s - \Delta_p \\ \Delta_s &= N_1\delta_s + N_0\gamma_s \\ \Delta_p &= N_1\delta_p + N_0\gamma_p. \end{aligned}$$

If no analyzer is placed after the fiber output, the transmitted fields represented in the ps reference system can be used to determine the intensity distribution. Hence, use of (A5) yields an output field

$$\tilde{E}_{\text{out}} = e^{j\Delta_p} \begin{pmatrix} |r_p|^{N_1} E_{p0} \\ |r_s|^{N_1} e^{j\Delta} E_{s0} \end{pmatrix} \tag{A6}$$

where E_{p0} and E_{s0} are the input E-field components in the ps system. The output intensity distribution is proportional to the function

$$F(\theta,\phi)=\tilde{E}_{\text{out}}^{\dagger}\tilde{E}_{\text{out}} \tag{A7}$$

with $\tilde{E}_{\text{out}}^{\dagger}$ representing the Hermitian conjugate of the column vector $\tilde{E}_{\text{out}}$.

For an unpolarized input field, $|E_{p0}|=|E_{s0}|=E_0$ and (A7) with the help of (A6) yields

$$F_{uu}(\theta)=\left[|r_p|^{2N_1}+|r_s|^{2N_1}\right]E_0^2. \tag{A8}$$

If the input field is x-polarized so that $E_{x0}=E_0$, the intensity distribution can be determined by use of the transformations (A1) and (A6) yielding

$$F_{pu}(\theta,\phi)=\left[|r_p|^{2N_1}(\cos\phi)^2+|r_s|^{2N_1}(\sin\phi)^2\right]E_0^2. \tag{A9}$$

If an analyzer is placed after the fiber output, the x-polarized input field is first transformed to the ps system by use of (A1), transmitted to the output according to (A6) and transformed back to the xy system at the output by inverting the transformation relation (A1). Using (A7), one obtains an intensity distribution given by

$$F_{pp}(\theta,\phi)=\Big[(\cos\phi)^4|r_p|^{2N_1}+(\sin\phi)^4|r_s|^{2N_1}+2(\sin\phi\cos\phi)^2\cos\Delta\Big]|E_0|^2. \tag{A10}$$

For a very long fiber, the number of reflections N_0 is large. Under this condition, the third term in the sum of the previous expression can be shown to average down to zero. To prove this, one considers the contribution to the intensity at an angle θ_0 as due to the sum of field components within a narrow range $\delta\theta$ around that angle. This average field is thus proportional to the quantity

$$f=\frac{1}{\delta\theta}\int_{\theta_0-\delta\theta/2}^{\theta_0+\delta\theta/2}e^{j\Delta}d\theta.$$

Given that

$$\Delta=N_1(\delta_s-\delta_p)+N_0(\gamma_s-\gamma_p)$$

for $\delta\theta\ll\theta_0$, the phase shifts all have an almost linear variation relative to the angle θ. Thus, to first order, the phase parameter Δ is approximately

$$\begin{aligned}\Delta&=N_1(a+b\theta)+N_0(c+d\theta)\\&=(N_1a+N_0c)+(N_1b+N_0d)\theta\end{aligned}$$

where a, b, c, and d are constants. Under this approximation,

$$f=e^{j(N_1a+N_0c)}e^{j(N_1b+N_0d)\theta_0}\frac{\sin\left[(N_1b+N_0d)\dfrac{\delta\theta}{2}\right]}{\left[(N_1b+N_0d)\dfrac{\delta\theta}{2}\right]}.$$

In practice, $N_0\gg N_1$, and for a very long fiber the condition, $(N_1b+N_0d)\,\delta\theta\gg 1$ is satisfied. Therefore, $|f|\ll 1$ and, thus, the contribution of the last term within brackets of (A10), is negligible. A similar development can be used to show that, for unpolarized input, the intensity distribution transmitted through an x-analyzer placed at the fiber output satisfies the property $F_{up}=F_{pu}$, with F_{pu} given by (A9) or, equivalently,

$$F_{up}(\theta,\phi)=\left[|r_p|^{2N_1}(\cos\phi)^2+|r_s|^{2N_1}(\sin\phi)^2\right]E_0^2. \tag{A11}$$

For a Gaussian beam focused to the center of the input fiber surface, one can use (9) in place of E_0^2 in (A8)–(A11).

REFERENCES

[1] M. T. Flanagan and R. H. Pantell, "Surface plasmon resonance and immunosensors," *Electron. Lett.*, vol. 20, no. 23, pp. 968–970, Nov. 1984.

[2] E. Kretschmann, "Determination of optical constants of metals through the stimulation for surface plasma oscillations" (in German), *Z. Phys.*, vol. 241, no. 4, pp. 313–324, 1971.

[3] E. Fontana, R. H. Pantell, and S. Strober, "Surface plasmon immunoassay," *Appl. Opt.*, vol. 29, no. 31, pp. 4694–4704, Nov. 1990.

[4] S. Sjolander and C. Urbanicczky, "Integrated fluid handling system for biomolecular interaction analysis," *Anal. Chem.*, vol. 63, no. 20, pp. 2336–2345, Oct. 1991.

[5] R. C. Jorgenson and S. S. Yee, "A fiber-optic sensor based on surface plasmon resonance," *Sens. Actuators B, Chem.*, vol. 12, no. 3, pp. 213–220, Apr. 1993.

[6] H. Murata, *Handbook of Optical Fibers and Cables*. New York: Marcel Dekker, 1988, pp. 41–42.

[7] J. H. Weaver, "Optical properties of metals," in *Handbook of Chemistry and Physics*, 71st. ed, D. R. Kudem, Ed. Boca Raton, FL: CRC Press, 1991, pp. 1287–1302.

[8] A. E. Siegman, *Lasers*, 1st ed. Stanford, CA: Univ. Sci. Books, 1986, pp. 665–666.

Eduardo Fontana was born in Rio de Janeiro, Brazil, in 1957. He received the B.Sc. degree in electrical engineering and the M.Sc. degree in physics from the Federal University of Pernambuco, Recife PE, Brazil, in 1980 and 1983, respectively, and the Ph.D. degree in electrical engineering from Stanford University, Stanford, CA, in 1989.

He is currently an Associate Professor in the Electronics and Systems Department, Federal University of Pernambuco. His past research activities have included microwave ferrite devices, low-temperature magnetic materials, magnetic semiconductors, optics, and free-electron lasers. His current research activities concern the use of surface plasmon spectroscopy in thin-film technology, integrated optics devices, and the development of optical-fiber sensors.